Synthesis, Characterization, and Bonding of Two New Heteropolychalcogenides: α-$CsCu(S_xSe_{4-x})$ and $CsCu(S_xSe_{6-x})$

Casey C. Raymond and Peter K. Dorhout*

Department of Chemistry, Colorado State University, Fort Collins, Colorado 80523

Received December 22, 1995[⊗]

The Cs−Cu−Q (Q = S, Se) system has been investigated using copper metal, cesium chloride, and alkali-metal polychalcogenide salts under mild hydrothermal reaction conditions. Heteropolychalcogenide salts and mixtures of known polysulfide and polyselenide salts have been used as reagents. The reaction products contain the α-$CsCuQ_4$ and $CsCuQ_6$ structures. The α-$CsCuQ_4$ phase exhibits a smooth transition in lattice parameters from the pure sulfur to the pure selenium phases, based on Vegard's law. The $CsCuQ_6$ phase has been prepared as the pure sulfur analog and a selenium rich analog. The single-crystal structures of the disordered compounds α-$CsCuS_2Se_2$ ($P2_12_12_1$, $Z = 4$, $a = 5.439(1)$ Å, $b = 8.878(2)$ Å, $c = 13.762(4)$ Å) and $CsCuS_{1.6}Se_{4.4}$ ($P\bar{1}$, $Z = 2$, $a = 11.253(4)$ Å, $b = 11.585(2)$ Å, $c = 7.211(2)$ Å, $\alpha = 92.93°$, $\beta = 100.94°$, $\gamma = 74.51°$) have been solved using a correlated-site occupancy model. These disordered structures display a polychalcogenide geometry in which the sulfur atoms prefer positions that are bound to copper. The optical absorption spectra of these materials have been investigated. The optical band gap varies as a function of the sulfur−selenium ratio. Extended Hückel crystal orbital calculations have been performed to investigate the electronic structure and bonding in these compounds in an attempt to explain the site distribution of sulfur and selenium.

Introduction

Several recent reviews have addressed the important field of metal chalcogenides,[1] in particular, the metal polychalcogenides.[2−4] Most of the polychalcogenides reported have contained either sulfur, selenium, or tellurium homoatomic anions (see for example refs 5−8). Only recently, have groups begun to explore heteropolychalcogenides as useful ligands for synthesis of new materials.[9−13] For most metal chalcogenide materials the electronic band gap lies between 0.3 and 3.0 eV, a feature important for optoelectronics. We have recently explored the effects of pressure on the band gap of $CsCuS_6$, demonstrating that the band gap in this compound displays a remarkably large pressure dependence.[14] It has been postulated that "internal" pressure in systems such as this may be applied by elemental substitutions. In this paper, we discuss our synthetic and theoretical exploration into the tunability of the structure and the optical band gap of ternary metal heteropolychalcogenides, α-$CsCuS_xSe_{4-x}$ and $CsCuS_xSe_{6-x}$, two quasi-infinite chain compounds.

Experimental Section

General Synthesis. Copper metal (99.9%) was obtained from Aesar. Cesium chloride (99.9%) was purchased from Fisher. Sulfur pieces and selenium shot (99.999%) were purchased from Johnson Matthey. All reagents were stored in a nitrogen filled glovebox and used without further purification. Deoxygenated water was prepared by purging deionized water with N_2 for several hours, prior to use. A_2Q_x (A = Na, K; Q = S, Se; $x = 1-6$) compounds were prepared via liquid ammonia synthesis as described previously.[15] All manipulations were performed with a nitrogen filled glovebox and standard Schlenk techniques. Yields were generally better than 80% based on copper metal as determined by powder X-ray diffraction.

Preparation of $Na_2S_3Se_3$. Na (0.6045 g, 26.3 mmol), S (1.2689 g, 39.6 mmol), and Se (3.1575 g, 40.0 mmol) were weighed into a Schlenk flask and sealed under nitrogen. The flask was connected to a Schlenk line and placed in an 2-propanol−dry ice bath at −60 °C. Anhydrous ammonia gas was then condensed into the flask, after drying over sodium turnings, and the mixture allowed to stir for 5 h. The NH_3 was evaporated and the products were left under vacuum overnight. DSC confirmed the existence of a single phase, with a melting point of 330 °C.

Preparation of α-$CsCuS_xSe_{4-x}$ (1). A representative reaction follows: Cu powder (31.9 mg, 0.5 mmol), K_2S_6 (131.9 mg, 0.5 mmol), and K_2Se_4 (192.0 mg, 0.5 mmol) were placed in a quartz ampule with 500 μl of 2 M CsCl aqueous solution. The ampule was evacuated (<1 mTorr) and flame sealed. The ampule was placed in a programmable furnace and heated to 150 °C, at 10 °C/h, for 24 h and cooled to 30 °C at 10 °C/h. The ampule was opened, vacuum filtered, and washed with water in air to remove unreacted polychalcogenide salts. Dark red needlelike crystals were obtained in high yields (based on the lack of copper metal starting material and the absence of other phases) and some Se metal was observed by powder X-ray diffraction. EDS data collected on the polycrystalline samples confirmed the presence of S and Se in the crystals. The approximate ratios were 1:1.1:2.2:2.8 = Cs:Cu:S:Se. Samples of **1** can be prepared with various *x*-values using appropriate mixtures of K_2S_4 and K_2Se_4.

* Author to whom correspondence should be addressed. Fax: 970-491-1801. E-mail: PKD@LAMAR.COLOSTATE. EDU.

⊗ Abstract published in *Advance ACS Abstracts,* August 15, 1996.

(1) Eichhorn, B. W. In *Progress in Inorganic Chemistry*; Karlin, K. D., Ed.; John Wiley & Sons Inc: New York, 1994; Vol. 42; p 139.
(2) Kanatzidis, M. G. *Chem. Mater.* **1990**, *2*, 353.
(3) Kanatzidis, M. G.; Huang, S. P. *Coord. Chem. Rev.* **1994**, *130*, 609.
(4) Kolis, J. W. *Coord. Chem. Rev.* **1990**, *105*, 195.
(5) Park, Y.; Liao, J.-H.; Kim, K.-W.; Kanatzidis, M. G. In *Inorganic and Organometallic Oligomers and Polymers*; Harrod, J. F., Laine, R. M., Eds.; Kluwer: Amsterdam, 1991; p 263.
(6) Kanatzidis, M. G.; Park, Y. *J. Am. Chem. Soc.* **1989**, *111*, 3767.
(7) Hartig, N. S.; Dorhout, P. K.; Miller, S. M. *J. Solid State. Chem.* **1994**, *113*, 88.
(8) Raymond, C. C.; Dorhout, P. K.; Miller, S. M. *Inorg. Chem.* **1994**, *33*, 2703.
(9) McCarthy, T. J.; Zhang, X.; Kanatzidis, M. J. *Inorg. Chem.* **1993**, *32*, 2944.
(10) Zhang, X.; Kanatzidis, M. G. *J. Am. Chem. Soc.* **1994**, *116*, 1890.
(11) Zhang, X.; Kanatzidis, M. G. *Inorg. Chem.* **1994**, *33*, 1238.
(12) Bollinger, J. C.; Ibers, J. A. *Inorg. Chem.* **1995**, *34*, 1859.
(13) Stevens, R. A.; Raymond, C. C.; Dorhout, P. K. *Angew. Chem., Int. Ed. Engl.* **1995**, *34*, 2509.
(14) Lorenz, B.; Orgzall, I.; Raymond, C. C.; Dorhout, P. K.; D'Adamo, R.; Hochheimer, H. D. *J. Phys. Chem. Solids* **1996**, *57*, 405.
(15) Liao, J.-H.; Kanatzidis, M. G. *Inorg. Chem.* **1992**, *31*, 431.

S0020-1669(95)01637-5 CCC: $12.00

Preparation of $CsCuS_6$ (2). Method A. Cu powder (31.6 mg, 0.5 mmol) and K_2S_5 (238.9 mg, 1.0mmol) were placed in a quartz ampule with 500 μL of 2 M CsCl aqueous solution. The ampule was evacuated (< 1 mTorr) and flame sealed. The ampule was placed in a programmable furnace and heated to 150 °C, at 10 °C/h, for 120 h and cooled to 30 °C at 20 °C/h. The ampule was opened, vacuum filtered, and washed with water in air. Orange plate-like crystals were isolated and the structure was confirmed with powder X-ray diffraction, CuS was also present. A similar reaction using K_2S_6 resulted in the same products.

Method B. Cu powder (159.0 mg, 2.5 mmol), K_2S_6 (1337.2 mg, 5.1 mmol), and CsCl (847.3 mg, 5.0 mmol) were weighed into a Schlenk flask. Upon addition of 20 mL of deoxygenated water to the flask, the mixture was allowed to stir at room temperature for 20 h, and a blood red precipitate was observed. The reaction was opened, filtered, and washed with water in air. Powder X-ray diffraction confirmed the presence of **2**. Total yield: 732.3 mg; 75% based on copper.

Preparation of $CsCuS_xSe_{6-x}$ (3). Cu powder (34.6 mg, 0.54 mmol) and $Na_2S_3Se_3$ (385.7 mg, 1.02 mmol) were placed in a quartz ampule with 500 μL of 2 M CsCl aqueous solution. The ampule was evacuated (<1 mTorr) and flame sealed. The ampule was placed in a programmable furnace and heated to 150 °C, at 10 °C/h, for 48 h and cooled to 30 °C at 10 °C/h. The ampule was opened, vacuum filtered, and washed with water in air. Black-red, lustrous plates were obtained, with similar crystal morphology as for **2**. EDS on the crystals confirmed the presence of S and Se in the crystal and no potassium was detected. The approximate ratios detected were 1:1.4:1.2:7.6 = Cs:Cu:S:Se.

Physical Characterization. Powder X-ray diffraction was performed with an Enraf-Nonius 601 generator and Guinier camera; powder patterns were indexed using U-Fit.[16] Single-crystal X-ray diffraction was performed on a Siemens P4 four-circle diffractometer using graphite-monochromated Mo Kα radiation. Energy dispersive spectroscopy (EDS) was performed with a Philips 505 SEM equipped with a Kevex detector and analysis software. Differential scanning calorimetry (DSC) was performed with a DuPont 9900 computer/thermal analyzer equipped with a 910 DSC module. UV/vis/near-IR diffuse reflectance spectra were recorded with a Hitachi U-3501 spectrophotometer equipped with a 60 mm diameter integrating sphere accessory and samples mounted on MgO plates.

Extended Hückel Calculations. The calculations were performed with PC versions of EHMACC and EHPC.[17] All calculations were performed with the asymmetric electronic unit, which in all cases was twice the crystallographic asymmetric unit. These units are shown as the cross-hatched atoms in Figure 1. The crystallographic information has previously been reported for α-$CsCuS_4$,[18] β-$KCuS_4$,[6] α-$CsCuSe_4$,[7] and $CsCuS_6$.[9] The 1-dimensional chains in all of these structures were propagated to three nearest neighbors. The calculation of CuQ_4^- compounds were performed over 20 *k*-points, while CuQ_6^- compounds were calculated over 5 k-points.[19] The energy values and Slater-type orbital exponents are given in Table 1.[20−22] Cesium was not included in the calculations due to a lack of reasonable orbital parameters; consequently, the absolute energy values and band gaps resulting from the calculations are not entirely accurate, but the *relative* orbital interactions, charges, and Fermi levels are reliable.

Results

General Single-Crystal X-ray Analysis. Rotation photos were used to determine the diffracting capability of single crystals of the title compounds. The unit cells were determined from at least 40 centered reflections, between 10−25° 2θ. Axial photographs confirmed the axial lengths and the Laue classes. Redundant data were collected in both cases (by a $\theta-2\theta$ scan out to 67°). A full quadrant was collected in both cases ($\pm h$, $\pm k$, $+l$). For $CsCuS_2Se_2$, 2647 reflections (1175 independent) were collected and 75 parameters refined. For $CsCuS_{1.6}Se_{4.4}$, 5383 reflections (4412 independent) were collected and 193 parameters refined. Semi-empirical absorption corrections (based on ψ-scans) were applied to the data. Both crystal structures were solved with direct methods and refined with SHELXTL, using full-matrix least-squares methods on F^2.[23]

On the basis of the unit cell parameters and the EDS data, the structures were expected to contain both S and Se. Initial refinements were used assuming a "pure" system, such as $CsCuS_4$ or $CsCuS_6$. This resulted in unstable models and erroneous thermal ellipsoids. In order to stabilize the solution a correlated site-occupancy model[12] was utilized. This was accomplished by constraining the Cu−Q and specific Q−Q bond distances, based on known structures,[6,7,9,18] and fixing the total site occupancy of each chalcogen position to 1.0. Only Se positions were allowed to refine anisotropically, while S positions were fixed at an isotropic value determined from initial isotropic refinements. Attempts were made to refine the Debye−Waller parameters with no improvement in the model. It was found in this way that the best isotropic values to use for sulfur were 0.038 and 0.020 for $CsCuQ_4$ and $CsCuQ_6$,

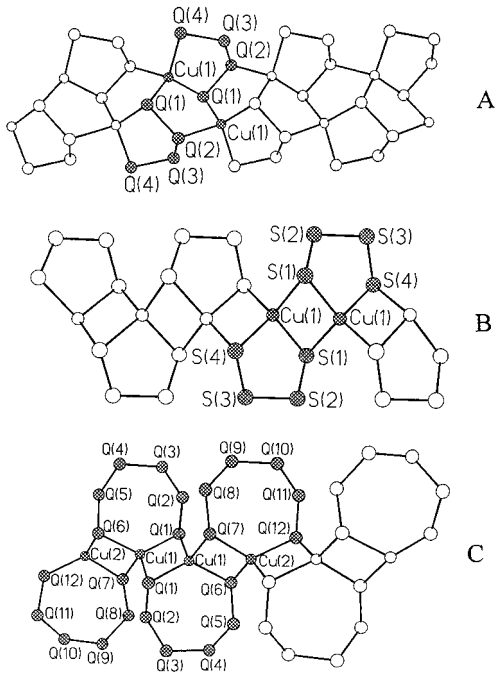

Figure 1. Anionic chain structures of (A) α-CuQ_4^-, (B) β-CuQ_4^-, and (C) CuQ_6^-. The asymmetric units used for the Extended Hückel calculations are highlighted with cross-hatching.

Table 1. Extended Hückel Parameters: Orbital Exponents (Coefficients) and Effective Potentials (eV)

atom, orbital	ζ (C)	ζ' (C')	H_{ii}	ref
S, 3s	2.122		−20.0	20, 21
3p	1.827		−13.3	
Se, 4s	2.43		−21.5	20
4p	2.07		−13.0	
Cu, 4s	2.20		−6.490	22, 31
4p	2.20		−3.359	
3d	6.676(0.487)	2.768(0.657)	−13.367	31

(16) Evain, M. *U-FIT: A cell parameter refinement program*; I.M.N.: Nantes, France, 1992.
(17) Whangbo, M.-H.; Evain, M.; Hughbanks, T.; Kertesz, M.; Wijeyeskera, S.; Wilker, C.; Zheng, C.; Hoffmann, R. *QCPE* **1989**, *9*, 61.
(18) Raymond, C. C.; Dorhout, P. K.; Miller, S. M. *Z. Kristallogr.* **1995**, *210*, 776.
(19) CuS_6^- could be computed with 20 *k*-points and these results were compared with a calculation over 5 *k*-points with no significant differences. Thus, all calculations for CuQ_6^- were perfomed over 5 *k*-points.
(20) Clementi, E.; Roetti, C. *At. Data Nucl. Data Tables* **1974**, *14*, 177.
(21) Chen, M. M. L.; Hoffmann, R. *J. Am. Chem. Soc.* **1976**, *98*, 1647.
(22) Hay, P. J.; Thibeault, J. C.; Hoffmann, R. *J. Am. Chem. Soc.* **1975**, *97*, 4884.
(23) Sheldrick, G. M. *J. Appl. Crystallogr.*, manuscript in preparation.

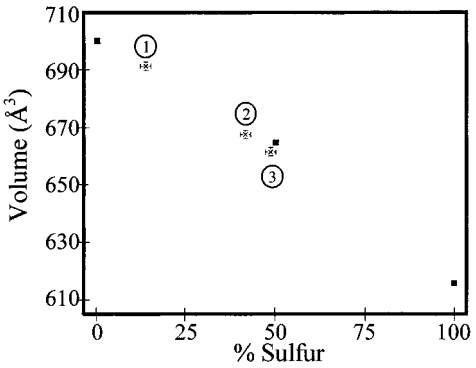

Figure 2. Vegard's law plot for α-$CsCuQ_4$, the solid squares (■) represent data and esd's determined from single-crystal X-ray structures. The points 1−3 represent data determined from powder diffraction for different ratios of K_2S_4/K_2Se_4: (1) 0.25 mmol:0.75 mmol, (2) 0.50 mmol:0.5 mmol, (3) 0.75 mmol:0.25 mmol.

Table 2. Crystallographic Parameters for α-$CsCuS_2Se_2$ and $CsCuS_{1.6}Se_{4.4}$

	α-$CsCuS_2Se_2$	$CsCuS_{1.6}Se_{4.4}$
fw	418.49	595.29
space group (No.), *Z*	$P2_12_12_1$ (19), 4	$P\bar{1}$(2), 2
a, Å	5.4390(10)	11.253(4)
b, Å	8.878(2)	11.585(2)
c, Å	13.762(4)	7.211(2)
α, deg	90.0	92.93(2)
β, deg	90.0	100.94(2)
γ, deg	90.0	74.51(2)
V, Å^3	664.5(3)	889.5(4)
T, °C	20	−110
λ, (Mo Kα), Å	0.71073	0.71073
D_{calc}, g cm^{-3}	4.183	4.445
μ, mm^{-1}	20.131	24.786
R_1[a]	0.0395	0.0744
wR_2[b,c]	0.0919	0.1962

[a] $R_1 = \sum||F_o| - |F_c||/\sum|F_o|$. [b] $wR_2 = [\sum w(F_o^2 - F_c^2)^2/\sum w(F_o^2)^2]^{1/2}$. [c] $w^{-1} = [\sigma^2(F_o^2) + (zP)^2]$ where $P = (F_o^2 + F_c^2)/3$, and $z = 0.0512$ and 0.124, respectively.

respectively. All correlations between the sulfur and selenium Debye−Waller parameters were found to be less than 0.95 in the final, full refinement.

Final refinements were performed without the bond length constraints, with no effect on the refinement parameters. More organized structures, S−Se−Se−S or S−Se−S−Se, were investigated, but all resulted in worse and less stable models. The structure of α-$CsCuQ_4$ crystallized in the noncentrosymmetric space group $P2_12_12_1$, and the Flack parameter[24,25] was investigated to determine the correct enantiomorph. The value of the Flack parameter was found to lie near 0.5; thus an absolute structure could not be determined. The structure was treated as a racemic twin, with a final absolute structure value of 0.41(7).

$CsCuQ_4$. The series of compounds has been prepared by combining Cu metal, CsCl, K_2Se_4 and K_2S_x ($x = 4, 6$). Copper metal and polyselenides, Se_y^{2-}, are oxidized as evidenced in the products, Cu(I) and Se metal. The structures of $CsCu(S_xSe_{4-x})$, ($0 \le x \le 4$), have been evaluated by single-crystal and powder X-ray diffraction, and there appears to be a smooth transition in lattice parameters from the pure sulfide ($x = 4$) to the pure selenide ($x = 0$). This is demonstrated in the Vegard's law plot, Figure 2. The points, 1−3, represent different starting ratios of K_2S_4 and K_2Se_4; EDS data obtained from the crystalline material support these S:Se ratios. The lattice parameters were determined from the powder diffraction data. At least 20 reflections were indexed and all *R*-values were less than 4.4%. Although there is a series of compounds that can be prepared for ($0 \le x \le 4$), there appears to be several "preferred" phases that are rich in selenium (see points 1−3 in Figure 2).

The single-crystal X-ray structure of one sample with the composition $CsCuS_2Se_2$ displayed a preference for the site occupations of the chalcogenides; however, there does not appear to be a preferred arrangement in the four-membered

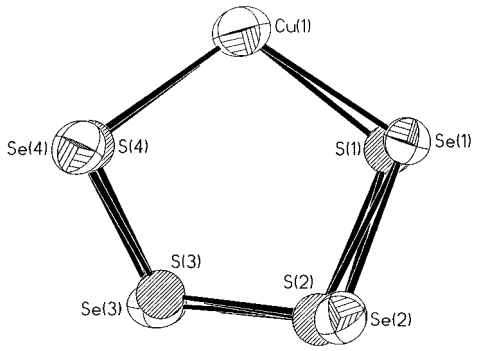

Figure 3. Crystallographic unique portion of α-$CsCuS_2Se_2$, with chalcogen positions labeled. The expanded view of the asymmeteric unit is shown with 50% probability thermal ellipsoids for copper and selenium; isotropic sulfur atoms are represented with striped circles.

Table 3. Final Positional Parameters, Isotropic Thermal Parameters[a] (*U*(eq) Fixed for All Sulfur), and Site Occupancy Factors

	Wyckoff letter	*x*	*y*	*z*	*U*(eq)	SOF
		A. α-$CsCuS_2Se_2$				
Cs(1)	4a	0.1596(2)	0.4357(1)	0.6672(1)	0.059(1)	1.00
Cu(1)	4a	0.0419(3)	0.3617(2)	0.9427(1)	0.050(1)	1.00
Se(1)	4a	0.364(2)	0.1889(9)	0.9030(7)	0.041(2)	0.43(1)
S(1)	4a	0.372(4)	0.215(2)	0.905(1)	0.038	0.57(1)
Se(2)	4a	0.647(1)	0.3522(6)	0.8356(4)	0.041(1)	0.55(1)
S(2)	4a	0.649(4)	0.379(2)	0.848(1)	0.038	0.45(1)
Se(3)	4a	0.581(1)	0.579(1)	0.9261(8)	0.051(1)	0.66(1)
S(3)	4a	0.558(7)	0.569(5)	0.925(3)	0.038	0.34(1)
Se(4)	4a	0.170(3)	0.615(2)	0.901(1)	0.046(3)	0.36(1)
S(4)	4a	0.178(4)	0.602(2)	0.913(1)	0.038	0.64(1)
		B. $CsCuS_{1.6}Se_{4.4}$				
Cs(1)	2i	0.8131(1)	0.4219(1)	0.3400(2)	0.024(1)	1.00
Cs(2)	2i	0.8082(1)	0.9258(1)	0.8250(2)	0.027(1)	1.00
Cu(1)	2i	0.0142(2)	0.6059(2)	0.0962(3)	0.028(1)	1.00
Cu(2)	2i	0.0018(2)	0.8738(2)	0.3453(4)	0.030(1)	1.00
Se(1)	2i	0.118(3)	0.413(2)	0.214(4)	0.024(2)	0.31(1)
S(1)	2i	0.111(3)	0.409(2)	0.202(5)	0.020	0.69(1)
Se(2)	2i	0.2867(2)	0.3529(1)	0.0717(3)	0.022(1)	0.926(6)
S(2)	2i	0.297(5)	0.367(4)	0.245(8)	0.020	0.074(6)
Se(3)	2i	0.4371(3)	0.4127(2)	0.2929(4)	0.026(1)	0.85(1)
S(3)	2i	0.445(5)	0.440(4)	0.277(7)	0.020	0.15(1)
Se(4)	2i	0.4393(3)	0.5930(3)	0.1688(4)	0.027(1)	0.85(1)
S(4)	2i	0.4118(4)	0.623(3)	0.197(6)	0.020	0.15(1)
Se(5)	2i	0.3023(3)	0.7311(3)	0.3199(4)	0.024(1)	0.81(1)
S(5)	2i	0.269(3)	0.749(3)	0.333(6)	0.020	0.19(1)
Se(6)	2i	0.113(2)	0.766(2)	0.115(4)	0.023(2)	0.50(1)
S(6)	2i	0.122(6)	0.754(5)	0.12(1)	0.020	0.50(1)
Se(7)	2i	−0.1106(7)	0.7277(6)	0.3133(6)	0.018(1)	0.54(1)
S(7)	2i	−0.108(2)	0.724(2)	0.348(3)	0.020	0.46(1)
Se(8)	2i	−0.2997(2)	0.7551(2)	0.4160(3)	0.020(1)	0.90(1)
S(8)	2i	−0.280(6)	0.735(5)	0.37(1)	0.020	0.11(1)
Se(9)	2i	−0.4370(2)	0.8965(2)	0.2022(3)	0.027(1)	0.96(8)
S(9)	2i	−0.36(1)	0.887(7)	0.18(1)	0.020	0.045(8)
Se(10)	2i	−0.4220(3)	0.0783(3)	0.3456(6)	0.026(1)	0.91(1)
S(10)	2i	−0.394(9)	0.07(1)	0.36(2)	0.020	0.09(1)
Se(11)	2i	−0.2934(6)	0.1459(5)	0.1828(5)	0.022(1)	0.87(1)
S(11)	2i	−0.30(1)	0.14(1)	0.15(1)	0.020	0.13(1)
Se(12)	2i	−0.100(3)	0.083(2)	0.350(3)	0.021(3)	0.39(1)
S(12)	2i	−0.095(4)	0.074(4)	0.336(6)	0.020	0.61(1)

[a] *U*(eq) is defined as one-third the trace of the orthogonalized $\mathbf{U}_{ij}$ tensor.

(24) Flack, H. D. *Acta Crystallogr., A* **1983**, *39*, 876.
(25) Bernardinelli, G.; Flack, H. D. *Acta Crystallogr., A* **1985**, *41*, 500.

Table 4. Selected Bond Lengths (Å) and Angles (deg)

		A. α-$CsCuS_2Se_2$	
Cu−S1	2.39(2), 2.28(2)	Cu−Se1	2.393(9), 2.38(1)
Cu−S2	2.50(2)	Cu−Se2	2.606(6)
Cu−S4	2.30(2)	Cu−Se4	2.42(2)
S1−Cu−S1	110.1(5)	Se1−Cu−Se1	112.4(2)
S1−Cu−S2	125.9(6), 98.3(6)	Se1−Cu−Se2	117.0(3), 99.5(3)
S1−Cu−S4	123.1(6), 103.6(7)	Se1−Cu−Se4	120.2(4), 109.3(4)
S2−Cu−S4	97.2(6)	Se2−Cu−Se4	97.7(3)
S1−Se2−Se3−S4	50.2(2)		
Cs−S(av)	3.668(9)	S−S (av)	2.13(2)
Cs−Se(av)	3.580(7)	Se−Se (av)	2.328(7)
		S−Se (av)	2.23(1)
		B. $CsCuS_{1.6}Se_{4.4}$	
Cu1−S1	2.36(4), 2.35(3)	Cu1−Se1	2.47(3), 2.34(3)
Cu1−S6	2.33(7)	Cu1−Se6	2.40(3)
Cu1−S7	2.59(2)	Cu1−Se7	2.44(7)
Cu2−S6	2.44(5)	Cu2−Se6	2.38(2)
Cu2−S7	2.38(3)	Cu2−Se7	2.35(7)
Cu2−S12	2.46(4), 2.28(5)	Cu2−Se12	2.39(3), 2.36(2)
Cu1−Cu1	2.82(4)		
S1−Cu1−S1	107(1)	Se1−Cu1−Se1	108.4(9)
S1−Cu1−S6	123(2),115.57(2)	Se1−Cu1−Se6	123.4(9),114.4(9)
S1−Cu1−S7	114.7(8), 109.3(9)	Se1−Cu1−Se7	112.5(7), 111.1(6)
S6−Cu1−S7	87(1)	Se6−Cu1−Se7	84.8(4)
S6−Cu2−S7	90(2)	Se6−Cu2−Se7	87.3(6)
S6−Cu2−S12	129(2), 127(2)	Se6−Cu2−Se12	127.7(8), 124(1)
S7−Cu2−S12	123(1), 113(1)	Se7−Cu2−Se12	122.2(7), 118.5(7)
S12−Cu2−S12	82(2)	Se12−Cu2−Se12	82.0(9)
S1-Se2-Se3-Se4	97.6(7)	Se3-Se4-Se5-S6	92.6(7)
S7-Se8-Se9-Se10	86.3(4)	Se9-Se10-Se11-S12	91.9(2)
Cs-S(av)	3.66(2)	S-S (av)	2.14(3)
Cs-Se(av)	3.738(5)	Se-Se (av)	2.305(5)
		S-Se (av)	2.32(2)

chalcogenide chain such as S−Se−Se−S. The crystallographically unique portion of the structure of the $^1_\infty[Cu(S_xSe_{4-x})]^-$ chain is shown in Figure 3. Indeed, the chalcogenide positions, Q1-Q4, as defined in Figure 1A, are fractionally occupied by both sulfur and selenium. Because the bonding requirements for sulfur and selenium are different (bond angles and distances), it was necessary to model the disorder on the chalcogenide positions not on one mutual lattice site but rather on two different sites (i.e. S and Se are not isomorphic). These sites were found initially by restricting the bond distances for sulfur and selenium; thereafter, the sites were allowed to refine independently, with the constraint that the fractional occupations of the two sites be correlated. This resulted in a final refinement where the sulfur content of Q1 and Q4 was quite a bit more than at sites Q2 and Q3. The final relevant X-ray analysis data, atomic positions, and relevant bond distances and angles are found in Tables 2, 3A, and 4A.

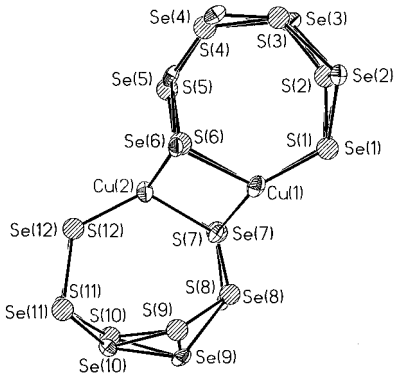

Figure 4. Crystallographic unique portion of $CsCuS_{1.6}Se_{4.4}$, with chalcogen positions labeled. The expanded view of the asymmeteric unit is shown with 50% probability thermal ellipsoids for copper and selenium; isotropic sulfur atoms are represented with striped circles.

$CsCuQ_6$. We found, as in the case of the $CsCuQ_4$ compound, that the site occupation of the chalcogenide atoms in $CsCuQ_6$ followed a similar trend. For example, a compound with the formula $CsCuS_{1.6}Se_{4.4}$, prepared by reacting $Na_2S_3Se_3$ with copper metal and CsCl, gave dark red anorthic plate crystals. Single-crystal X-ray diffraction showed a compound whose chalcogenide positions were again disordered; the crystallographically unique portion of the structure of the $^1_\infty[CuQ_6]^-$ chain is shown in Figure 4. We found, however, that there was a strong preference for sulfur in the Q1, Q6, Q7, and Q12 positions (see Figure 1C) in the unique portion of the unit cell. The final relevant X-ray analysis data, atomic positions, and relevant bond distances and angles are found in Tables 2, 3B, and 4B.

Discussion

Structures. It was found that there is a statistical distribution over all sites of both sulfur and selenium with sulfur dominating two distinct positions in each structure evaluated. As expected from chemical first principles, those two positions occur at the "ends" of the chalcogen chains in the structure. Since the bonding in α-$CsCuQ_4$ is not straightforward, it is not surprising that the distribution of sulfur over the four chalcogen sites is not simply S−Se−Se−S. It does follow rather nicely that the distribution in $CsCuS_{1.6}Se_{4.4}$ is simpler. Indeed, we find a prefered organization, based on site occupancies, for S−Se−Se−Se−Se−S.

Since the distribution of chalcogens exists over all sites in both structures, one must conclude that there are no "simple"

(26) We are currently investigating the speciation of these polychalcogenides in aqueous solutions by electrospray mass spectrometry. Raymond, C. C.; Dick, D.; Dorhout, P. K. in preparation. Raymond, C. C.; Dick, D.; Dorhout, P. K. Manuscript in preparation.

heteropolychalcogenides in solution, but rather that a distribution of heteropolychalcogenide fragments of differing chain lengths must exist.[26] There should exist, however, a probability distribution for finding a $Cu-SQ_n$ cluster fragment as well as a $Cu-SeQ_n$ cluster fragment in solution. The relative stability of these fragments toward dissociation should ultimately determine how frequently they appear in the structure. Given that the Cu−S and Cu−Se bond energies are nearly identical (~70 kcal/mol)[27] there may be other kinetic factors at work here.

For example, it is quite common to find disulfide and diselenide species in solids formed from solvatothermal reactions. Indeed, there are numerous examples of polyselenide and polysulfide chains and rings found in solids isolated from solvatothermal reactions.[3,4,28,29] There are very few, if any, examples of isolated 5-membered rings of either polysulfide or polyselenide. Although statistically probable, these rings are not found isolated in the solid state, nor was there any evidence that they existed in the distribution of sulfur and selenium in the chains in our solids.

For $CsCuS_2Se_2$, the structure forms in the α-$CsCuQ_4$ type with a distribution of sulfur over the four sites as listed in Table 3A. A view of the unique portion of the chain structure is seen in Figure 3, expanded to illustrate the distinct sulfur and selenium sites at each chalcogenide site along the chain. The site occupancy factors for each chalcogenide site were correlated to the pair (S, Se) that comprise the site.[12] This was done to account for the differences in bonding requirements for sulfur and selenium, especially metal−chalcogen and chalcogen−chalcogen bond distances.

In the $CsCuQ_4$ series of compounds, the unit cell parameters vary according to Vegard's law with chalcogenide content. This can be seen in Figure 2. A smooth curve could be drawn for the solid solutions that exist between the points determined from the single-crystal analysis (i.e. α-$CsCuS_4$, $CsCuS_2Se_2$, and $CsCuSe_4$), the black squares in Figure 2. Points 1−3 illustrate unit cell volumes derived from powder diffraction patterns and their corresponding fraction of sulfur over all Q-sites. It is clear from this curve that the compounds in the family $CsCu(S_xSe_{4-x})$ form a solid solution.

For $CsCuS_{1.6}Se_{4.4}$, a distribution of chalcogenides similar to the $CsCuQ_4$ family is found over Q1−Q12, with Q1, Q6, Q7, and Q12 being predominantly S-based. In fact, these four Q-sites are very sulfur rich, see Table 3B. The other sites, however, are very much dominated by selenium (>80%). A view of the unique portion of the structure is seen in Figure 4, again illustrating the distinct sulfur and selenium atoms at each site. The refinement of the single crystal data did not proceed as well as in the $CsCuS_2Se_2$ case above. The final electron density map was reasonably flat, but electron density (~2.9 e/Å^3) was found near Cs in several regions of the map. EDS did not suggest the presence of potassium in the structure, so no attempt was made to refine this density as a fractionally occupied potassium impurity. The weighting factor settled at an acceptable value (see Table 2), but only a ψ-scan absorption correction was applied to the data. Application of a secondary extinction to the refinement did not help. Finally, since the pure $CsCuSe_6$ salt is yet unknown, a Vegard's law plot could not be determined for this set of compounds; however, the trend of increasing volume with increasing selenium concentration in the structures was observed.

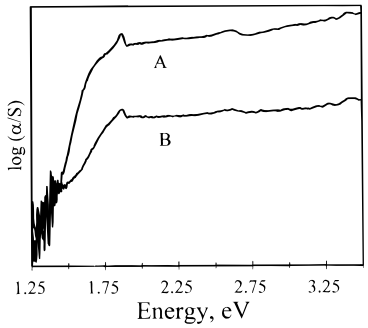

Figure 5. Diffuse reflectance spectra of (A) α-$CsCuSe_4$ and (B) α-$CsCuS_2Se_2$ plotted as log(α/*S*) vs energy, eV.

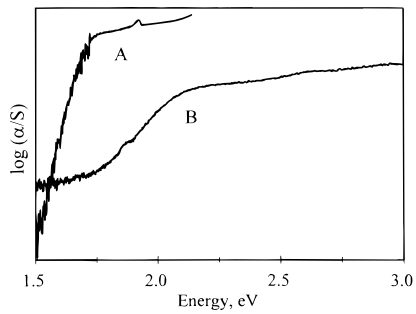

Figure 6. Diffuse reflectance spectra of (A) α-$CsCuS_{1.6}Se_{4.4}$ and (B) $CsCuS_6$ plotted as log(α/*S*) vs energy, eV.

Optical Spectroscopy. Diffuse reflectance spectra for the compounds shows a shift in the optical band gap of our heteropolychalcogenide compounds from 2.2 eV in the case of $CsCuS_4$ and $CsCuS_6$. The spectra of $CsCuSe_4$ (A) and $CsCuS_2Se_2$ (B) are shown Figure 5, plotted as log(α/*S*) vs energy after the Kubelka−Munk relationship for scattering solids.[30] From this plot we calculate an optical band gap of 1.3 eV for $CsCuSe_4$ and 1.5 eV for $CsCuS_2Se_2$. A similar plot of the spectra of $CsCuS_{1.6}Se_{4.4}$ (A) and $CsCuS_6$ (B) is shown in Figure 6, from which the optical band gap for $CsCuS_{1.6}Se_{4.4}$ was measured at 1.65 eV. From these examples, we can determine that an expected red-shift in the optical band gap accompanies the increase in the concentration of selenium.

Extended Huckel Calculations. The single electron calculation that has proven so useful in explaining structural preferences and physical properties was used to examine the buildup of charge on certain atomic positions and the overall bonding scheme in the compounds. We believed that a sound explanation for our observations in the $CsCuQ_x$ structures could be realized. For all of our calculations, the crystal structure parameters were employed and a large enough basis set was used to model the 1-dimensional translational symmetry in the unit cells. Ionization and orbital parameters were derived from charge-iterated compounds such as $TlCu_3S_2$;[31] all parameters used are listed in Table 1.

A. $CsCuQ_4$. A schematic representation of the α-$CsCuQ_4$ structure is shown in Figure 1A. The α-$CsCuQ_4$ and β-$KCuS_4$ phases are compared in this discussion since they are polytypes and their structures should have similar crystal orbitals. In the α-$CsCuS_4$ model, we observed that the charges built up on the sulfide sites as shown in Chart 1A and the charges on the sulfides in β-$KCuS_4$ built up as shown in Chart 1B. The charge distribution in the model selenide α-$CsCuSe_4$ is shown in Chart

(27) *CRC Handbook of Chemistry and Physics*, 60th ed.; Weast, R. C., Ed.; CRC Press: Boca Raton, FL, 1979; p F-222.
(28) Liao, J.-H.; Kanatzidis, M. G. *J. Am. Chem. Soc.* **1990**, *112*, 7400.
(29) Sheldrick, W. S.; Braunbeck, H. G. *Z. Naturforsch.* **1989**, *44B*, 1397.
(30) Wilkinson, F.; Kelly, G. In *CRC Handbook of Organic Photochemistry*; Scaiano, J. C., Ed.; CRC Press: Boca Raton, FL, 1989; Vol. 1; p 293.
(31) Berger, R.; Dronskowski, R.; Noren, L. *J. Solid State Chem.* **1994**, *112*, 120.

Chart 1

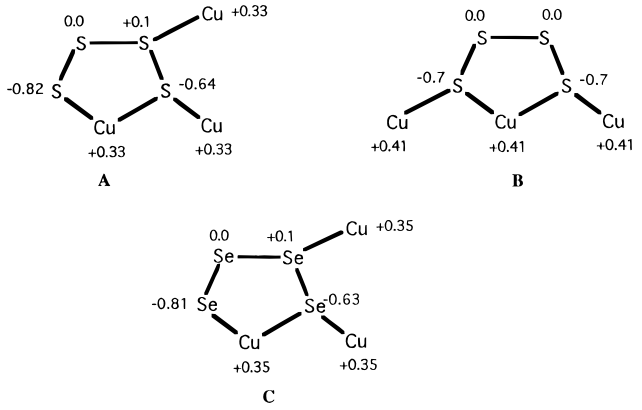

Chart 2

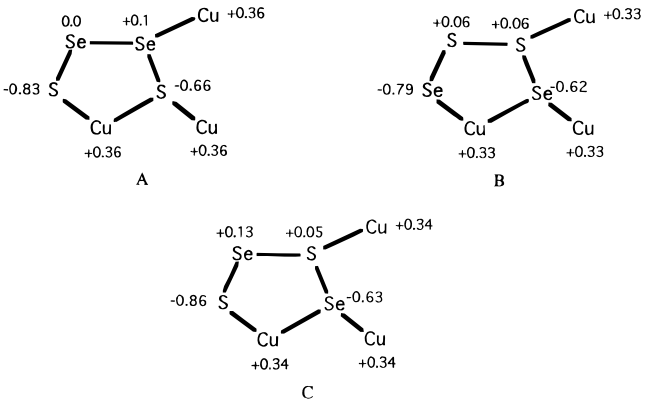

1C. These schemes demonstrate that the "ends" of the chains are more negative than the other positions and that these sites should contain a higher fraction of sulfur, based only on electronegativity arguments. Moreover, these charge distributions help rationalize the crystallographic model and the sulfur and selenium distribution over the different sites, Q1−4. In fact, calculations were performed on several model distributions of the chalcogenides S and Se for the α-$CsCuS_2Se_2$ compound, and these models are shown in Chart 2, together with their charges.

We have also prepared density of states (DOS) projections for the α- and *β*-forms of $ACuS_4$, shown in parts A and B of Figure 7. It should be noted that the highest occupied crystal orbital (HOCO) bands for both the α- and *β*-structures are dominated by sulfur t_2 (p-based) antibonding orbitals (assuming a T_d copper complex). The narrow copper bands lie lower than the band gap edge, in accord with the nearly (+1) charge on each and consistent with the valence band XPS spectra found for a series of copper sulfides and selenides.[32] The copper bands correspond to the t_2 and e set of d-orbitals found for nominally T_d copper sulfides. The a_1 and t_2 s- and p-based copper orbitals lie above the gap in the lowest unoccupied crystal orbitals (LUCOs) along with antibonding Q−Q orbitals. For α- and *β*-structures, the band gaps (observed, 2.2 eV) are consistent with the two materials. Indeed, there are only very subtle differences between these two compounds—the slightly larger Cu−S bonding component of the HOCO in the α-$CsCuS_4$, as indicated by the crystal orbital overlap population (COOP) curves shown in parts A and B of Figure 8 and the orbital representations shown in Chart 3.

It should be noted that in Chart 3, the interactions between orbitals 2 and 3 in the HOCO are a negative lobe on 2 to positive lobe on 3, since the two atoms are not coplanar in this orbital dimension.

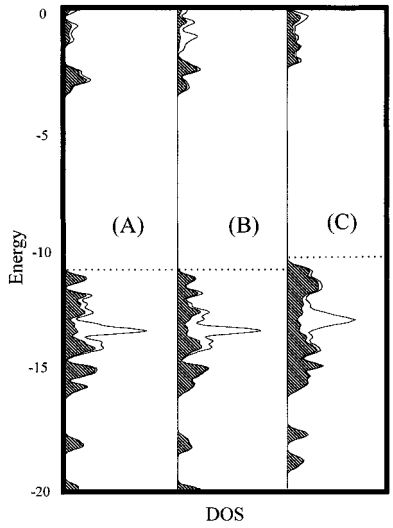

Figure 7. DOS curves: (A) α-$CsCuS_4$; (B) *β*-$KCuS_4$; (C) $CsCuS_6$. The Fermi level is indicated with a dashed line. The areas represent the contributions from sulfur (shaded) and copper (open).

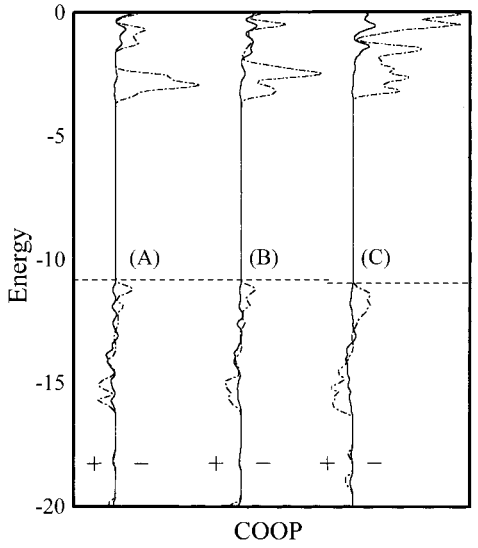

Figure 8. COOP curves: (A) α-$CsCuS_4$; (B) *β*-$KCuS_4$; (C) $CsCuS_6$. The Fermi level is indicated with a dashed line. The lines represent the following interactions: Cu−S (—) and S−S (— · —). The positive signs (+) indicate bonding interactions and the negative signs (−) indicate antibonding interactions.

Chart 3

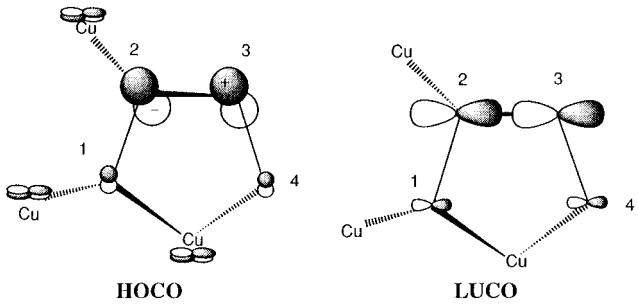

A comparison of the DOS and COOP curves for the α-phases of $CsCuS_4$, $CsCuS_2Se_2$, and $CsCuSe_4$ is shown in Figures 9 and 10. The particular chalcogenide arrangement for the $CsCuS_2Se_2$ chosen for our model is in Chart 2A. An initial glance shows the emergence of considerable Se contribution to both the HOCO and the LUCO states. In the $CsCuSe_4$ case, more

(32) Folmer, J. C. W.; Jellinek, F. *J. Less-Comm. Met.* **1980**, *76*, 153.

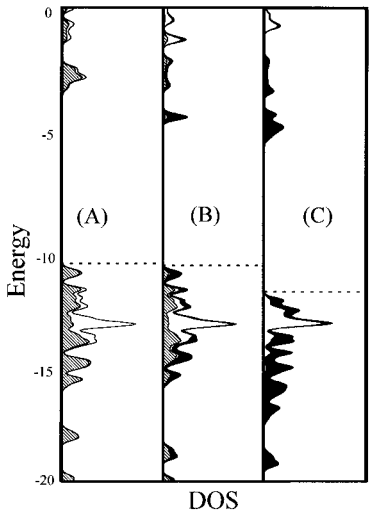

Figure 9. Density of states (DOS) curves: (A) α-$CsCuS_4$; (B) α-$CsCuS_2Se_2$; (C) α-$CsCuSe_4$. The Fermi level is indicated with a dashed line. The areas represent the contributions from sulfur (shaded), copper (open), and selenium (black). The ligand arrangement for S_2Se_2 is [S−Se−Se−S].

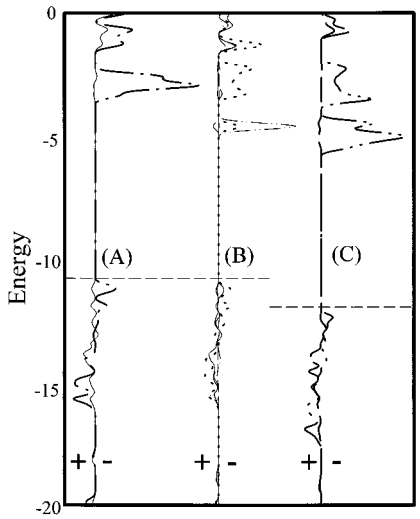

Figure 10. Crystal overlap population (COOP) curves: (A) α-$CsCuS_4$; (B) α-$CsCuS_2Se_2$; (C) α-$CsCuSe_4$. The ligand arrangement for S_2Se_2 is [S−Se−Se−S]. The Fermi level is indicated with a dashed line. The lines represent the following interactions: Cu−S (—), Cu−Se (- - -), Se−Se (— ·· -), and S−Se (···). The positive signs (+) indicate bonding interactions and the negative signs (-) indicate antibonding interactions.

Cu contribution begins to appear near the HOCO levels. A comparison of the COOP curves for the three examples is shown in Figure 10. For the $CsCuS_4$ and the chosen configuration of $CsCuS_2Se_2$, there is some bonding contribution from Cu−S interactions near the Fermi level. In $CsCuSe_4$, the Cu−Se bonding contribution is minimal if not zero. It is also important to note that the LUCO levels at the conduction band edge are predominantly Q−Q antibonding.

Traditionally, a comparison of total energies is made when evaluating the best structural configurations via Hückel calculations.[33−35] For our compounds, an evaluation of the total energies found that they differed by only 2% and not in any explainable manner (of course, the crystal lattice energies are not considered in the calculation and they also contribute to the stabilization of one particular configuration). Therefore, our only recourse in explaining the crystallographically observed distribution of chalcogenides was to examine the charges on each site (explained above), the distribution of selenium at the Fermi level, and the torsional Q1−Q2−Q3−Q4 angle.

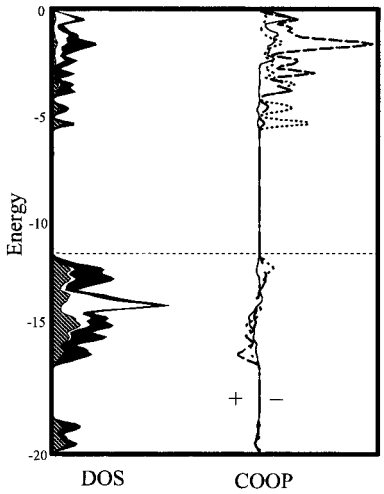

Figure 11. DOS and COOP curves for $CsCuS_2Se_4$ with a [S−Se−Se−Se−S] ligand arrangement. The Fermi level is indicated with a dashed line. The areas in the DOS curves represent the contributions from sulfur (shaded), copper (open), and selenium (black). The lines in the COOP curves represent the following interactions: Cu−S (—), Cu−Se (- - -), Se−Se (— ·· —), and S−Se (···). The positive signs (+) indicate bonding interactions and the negative signs (−) indicate antibonding interactions.

The HOCO level in the $CsCu(S_xSe_{4-x})$ family of solids investigated here is made primarily of the p-orbitals on the Q2 and Q3 sites in all examples. These sites develop zero or slightly positive charges, a condition more highly favored by selenium than sulfur as shown in their relative ionization potentials.[36] We also observed in the calculations that other arrangements of sulfur and selenium over the sites (Chart 2B, C) put more sulfur contribution into the HOCO level. Given the option, based on ionization potentials, sulfur would rather be buried deeper into the valence band. We conclude from the calculations that the preference for selenium in this structure is to occupy the Q2 and Q3 sites on the chain; a finding consistent with the crystallography.

Finally, after comparing total energies and illustrating that the more electronegative element, sulfur, prefers the chain terminal sites (a "general priciples" idea), we compared the torsional angles of the four-membered chalcogenide chain to known sulfide, selenide, and mixed chalcogenide chain and ring compounds.[3,4,28,29,37,38] For the S−Se−Se−S configuration, the torsional angle is 50.2(6)°, a bit acute for selenium chains, but more obtuse than the all-sulfur chain. Other configurations resulted in less-desireable angles. Based on these observations, we can conclude that the theoretical treatment of the distribution of sulfur and selenium over all the available sites resulted in a model that closely resembles that found crystallographically.

B. $CsCuQ_6$. As for the $CsCuQ_4$ family above, we used the Hückel calculations to develop a charge distribution over the atomic sites in the $CsCuQ_6$ structure. The distribution of charge over one link in the chain in $CsCuS_6$ is shown in **4**. The structure of $CsCuSe_6$ has not been reported, so there is no comparative DOS or COOP curves that would represent a real system. The DOS curve for $CsCuS_6$ was compared to the α-

(33) Zheng, C.; Hoffmann, R. *J. Am. Chem. Soc.* **1986**, *108*, 3078.
(34) Ortiz, J. V.; Hoffmann, R. *Inorg. Chem.* **1985**, *24*, 2095.
(35) Hughbanks, T.; Hoffmann, R. *J. Am. Chem. Soc.* **1983**, *105*, 1150.
(36) *The NBS Tables of Chemical Thermodynamic Properties*; American Chemical Society: Washington, DC, 1982; Vol. 11, p 392.
(37) Weiss, J.; Bachtler, W. *Z. Naturforsch.* **1973**, *28B*, 523.
(38) Pfitzner, A.; Zimmerer, S. *Z. Anorg. Allg. Chem.* **1995**, *621*, 969.

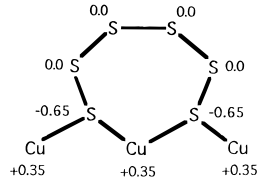

4

and β-$ACuS_4$ DOS curves in Figure 7C. As for α- and β-$ACuS_4$, the HOCO levels of $CsCuS_6$ are dominated by the Q1, Q2, Q5, Q6, Q7, Q8, Q11, and Q12 sulfur atoms, shown in **5**. The distribution of charges in $CsCuS_{1.6}Se_{4.4}$ is shown in

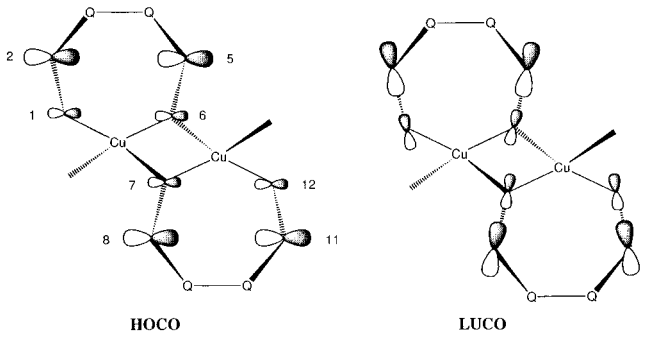

5

6. The DOS curve of $CsCuS_2Se_4$ for the S−Se−Se−Se−Se−S

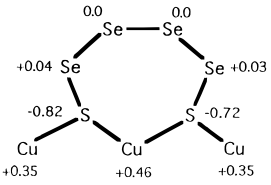

6

configuration in **6** is shown in Figure 11 with the COOP curve. The HOCO and LUCO are again dominated by Se t_2 contributions in this structure as they were for the $CsCuS_2Se_2$ configuration, see **5**, above. Although there is little charge buildup on Q2−5 and Q8−11, the more neutral, or slightly positive charge configuration is preferred for selenium than for sulfur. The COOP curves show that the orbitals near the Fermi level are mostly Q−Q antibonding. The LUCO orbitals are again chalcogen t_2 based and strongly antibonding in Q−Q. The orbital pictures are similar to those in **3**, with selenium atoms on Q2, Q5, Q8, and Q11 contributing the most to the antibonding Q−Q interactions.

Based on these observations, we have concluded that the driving force behind the arrangement of sulfur and selenium in $CsCuS_{1.6}Se_{4.4}$ is the preference for sulfur to sit on sites in the lattice that (1) develop the most negative charge and (2) are below the Fermi level. This confirmation, **6**, is also favored due to the ability of selenium to support the p-type charge carriers that dominate the conducting carriers at the Fermi level in most copper chalcogenides.

As we described for the $CsCuQ_4$ compounds above, we also evaluated the torsional angles in the Q_6 chain in $CsCuQ_6$. Angles generated from the S−Se−Se−Se−Se−S model for each end of the 6-membered chain are 97.6(6) and 92.6(6)°, respectively. Other ordering around the ring results in unrealistic (very acute) torsional angles. This observation, together with the charge distribution results discussed above, argues well for the observed crystal structure.

Conclusions

A series of mixed cesium copper sulfide−selenides has been prepared by hydrothermal synthesis having either the α-$KCuS_4$ or the $CsCuS_6$ structure. There appears to be a set of solid solutions of sulfur and selenium compounds that can be isolated depending on the type and relative ratios of polychalcogenides in the starting solutions. Single-crystal X-ray diffraction studies of two crystals showed that there is generally a preference for the quantity of sulfur or selenium at each chalcogenide site. The preferences have been examined and explained using the extended Hückel analysis of the quasi-infinite 1-dimensional chains of copper chalcogenides.

Acknowledgment. P.K.D. would like to acknowledge financial support from the Research Corporation, Cottrell Fellowship, and Colorado State University. We thank Professors T. Hughbanks and M.-H. Whangbo for helpful discussions. We also thank Susie Miller for crystallographic assistance and Catherine Zelenski for EDS.

Supporting Information Available: Tables of powder diffraction (*d*-spacing) data for $CsCuQ_4$ and $CsCuQ_6$ (3 pages). Two X-ray crystallographic files, in CIF format, are available. Access and/or ordering information is given on any current masthead page.

IC9516370